Probing Polymer Viscoelastic Relaxations with Temperature-Controlled Friction Force Microscopy

Jon A. Hammerschmidt and Wayne L. Gladfelter*

Department of Chemistry, University of Minnesota, Minneapolis, Minnesota 55455

Greg Haugstad

Center for Interfacial Engineering, University of Minnesota, Minneapolis, Minnesota 55455

Received December 22, 1998

ABSTRACT: A quantitative method, using temperature-controlled friction force microscopy (FFM), has been developed to determine the frictional (dissipative) character of thin polymer films. With this method variations in friction are sampled over micrometer-scale regions and are reduced to "friction histograms," yielding the distribution of frictional forces on the surface. The temperature dependence of the mean value of the frictional distribution is correlated to the known glass-to-rubber transition (T_g) and/or secondary relaxation mechanisms in films of poly(methyl methacrylate) (PMMA), poly(ethylene terephthalate) (PET), and polystyrene (PS). The dominant contribution to friction, on polymer films, was attributed to viscoelastic mechanical loss. Using equivalent time scales, measured T_g's were lower than bulk polymer values. The frictional response of PMMA displayed time−temperature equivalence upon variation of scan-velocity and temperature. The rate dependence of the hindered rotation of the $-COOCH_3$ group (β relaxation) in PMMA was consistent with Arrhenius type behavior, allowing calculation of an activation energy. The activation energy of the thin film was found to be lower than measured bulk energies.

Introduction

The importance of polymeric films as protective coatings, adhesives, lubricants, etc. has brought increased attention to polymer surface properties.[1,2] The behavior of a thin polymer film, not surprisingly, is known to vary considerably from that of the bulk polymer.[3] This is a result of chain conformation differences,[4] confinement effects,[5] and the effects of air−polymer and substrate−polymer interfaces dominating a large portion of the films.[6−8] Differences in free volume due to surface chain-end concentration can also impact polymer surface properties.[8−10] The combined thin film and surface effects have been shown to affect the polymer viscoelastic relaxation properties and therefore the tribological properties.

The tribological properties, in particular friction, of polymers are known to have a large, even dominant contribution from internal viscoelastic dissipation,[11] which ultimately is derived from molecular relaxation. Traditionally this was characterized by macroscopic measurements of rolling friction as a function of velocity and/or temperature.[11,12] These rolling friction experiments mapped out a response similar to bulk viscoelastic loss tangent (tan δ) data, an expected result considering the thick (>100 μm) polymer films and large probing depths employed.

With the emergence of friction force microscopy (FFM),[13] a type of scanning probe microscopy (SPM) that measures the lateral force on a probe caused by sliding friction, the ability to probe frictional processes at the nanometer scale is possible. Because the probe has a radius of curvature of tens of nanometers, and applied loads are on the nanonewton scale, the true surface layer can be studied under wearless sliding contact. Several studies have been made using the velocity dependence of friction to probe polymer molecular motion on thin films using FFM.[4,14−16] Gelatin, poly(vinyl alcohol) (PVOH), poly(vinyl acetate) (PVAc), poly(ethylene terephthalate) (PET), and polystyrene (PS) thin films exhibit peaks in the velocity dependence of friction, attributed to the glass-transition or secondary relaxations (reflecting movement of functional groups on polymer chains). The velocity dependence of friction on nominally dry gelatin films displayed a peak in the friction-velocity relationship, which was attributed to the glass-to-rubber transition (T_g).[14] The peak shifted to higher velocity for increasingly perturbative scanning. Variations in frictional distributions were also recorded. Friction histogram breadth and symmetry reflected the energy dispersion of relaxations characteristic of glassy or rubbery behavior. In another study an estimated contact diameter of the probe tip as a velocity-to-frequency conversion length scale allowed comparison to tabulated frequency-dependent tan δ data.[15] This enabled the assignment of the α and/or β relaxation processes for PET, PVOH, PVAc, and gelatin thin films. Kajiyama et al. investigated the rate dependence of friction by varying the molecular weight of polystyrene.[4] A transition from glassy to rubberlike behavior with decreased molecular weight was demonstrated, and was attributed to excess free volume at the surface induced by surface segregation of chain end groups.

One obstacle of the above experiments was the limited velocity range available in commercial FFM, typically 4 orders of magnitude. It is well-known that both the time scale and the temperature affect the overall viscoelastic behavior of a polymer system.[17] To date the limitations of *piezoelectric* scanners have restricted the range of temperatures examined to a narrow range near ambient conditions. With newly designed force microscopes, a broader range of temperature variation is now accessible. This provides a unique opportunity to explore

* To whom correspondence should be addressed.

10.1021/ma981966m CCC: $18.00
Published on Web 04/30/1999

both temperature- and time-dependent polymer relaxation phenomena.

In the present study, we strive to develop a molecular-scale understanding of friction on polymer film surfaces by examining temperature-dependent behavior, as well as the interplay between time (velocity) and temperature.

Experimental Section

Materials. PMMA (Polysciences, MW = 60 000, M_w/M_n = 1.10), PS (Aldrich, MW = 44 000, M_w/M_n = 1.10), and PET (Aldrich) films were prepared by spin coating (2000 rpm) 0.25 wt % polymer/solvent solutions onto silicon (100) wafers, which had a native oxide layer. Toluene was used as the solvent for PMMA and PS, and 2-chlorophenol was used for PET. Films were annealed at 100 °C under vacuum (≈0.01 Torr) for 2 h and allowed to cool under vacuum. Experiments were performed within days of film coating, and 1 day or less after annealing. Film thicknesses were measured using ellipsometry (Sopra) and found to be approximately 21, 12, and 20 nm (±5 nm), for PMMA, PET, and PS, respectively. Film surfaces were homogeneous with rms roughnesses ≤1 nm.

Instrumentation. All film characterization was performed with a PicoSPM (Molecular Imaging) scanning probe microscope with an M-scanner (lateral range = 30 μm; vertical range = 7 μm) in conjunction with a Nanoscope III controller (Digital Instruments). The design of the PicoSPM isolates the sample stage from the piezoelectric scanner and associated electronics, thus allowing for a wide variation in sample temperature, humidity, and atmosphere. Temperature variation is accomplished via a resistive heating stage (temperature range: ambient temperature to 170 °C). The temperature stage was calibrated using a k-type microthermocouple attached to a bare Si(100) wafer. The stage temperature response was linear throughout its range, and reached each set temperature within approximately 5 min. The sample area was enclosed within an O-ring-sealed glass chamber. A $CaSO_4$ column in conjunction with a hygrometer and feedback-controlled airflow were used to control the relative humidity (RH) for all experiments between 2 and 8%, limiting the effect of adsorbed water on the surfaces. Polymer films were equilibrated at these humidities for several hours before collecting images. Commercial uncoated 85-μm silicon cantilevers (spring constant ≈ 0.5 N/m) with integrated sharpened tips (Park Scientific Instruments) were used to characterize the frictional behavior of the polymer films. Reflective coatings were precluded in order to eliminate cantilever bending due to the difference in thermal expansivity of the cantilever and coating material. The probe tip radius of curvature was characterized through the use of a calibration grating (NTMDT). The grating is composed of silicon needles with a radius of curvature of <10 nm. Figure 1a displays a topographic image of one grating needle acquired in contact mode, and rendered as a surface plot. Figure 1b shows a profile of the tip apex from Figure 1a. The topographic profile obtained is a convolution of the grating and probe tip radius of curvatures (r_c).[18,19] From the image profile r_c = 26.8 nm, containing the sum of tip and grating radii of curvatures. The nominal radius of curvature from the manufacture was approximately 20 nm, in agreement with our measurement given <10 nm contribution from the calibration grating. The radius of curvature for the probe tip used in these experiments was therefore estimated at ≈20 nm. Frictional measurements will depend on the precise shape of the probe tip. In all measurements penetration depths are only several nanometers, where the probe tip is shown to be spherical. This issue will be addressed further in the discussion section.

Procedures. Figure 2 (top) displays three images which were acquired simultaneously, topography (height), friction (trace), and friction (retrace) on a PMMA surface. Height images were acquired to determine surface roughness and wear and to gauge any topographic contributions to the lateral force. Forces remained sufficiently low to preclude changes in the measured topography over the course of an experiment;

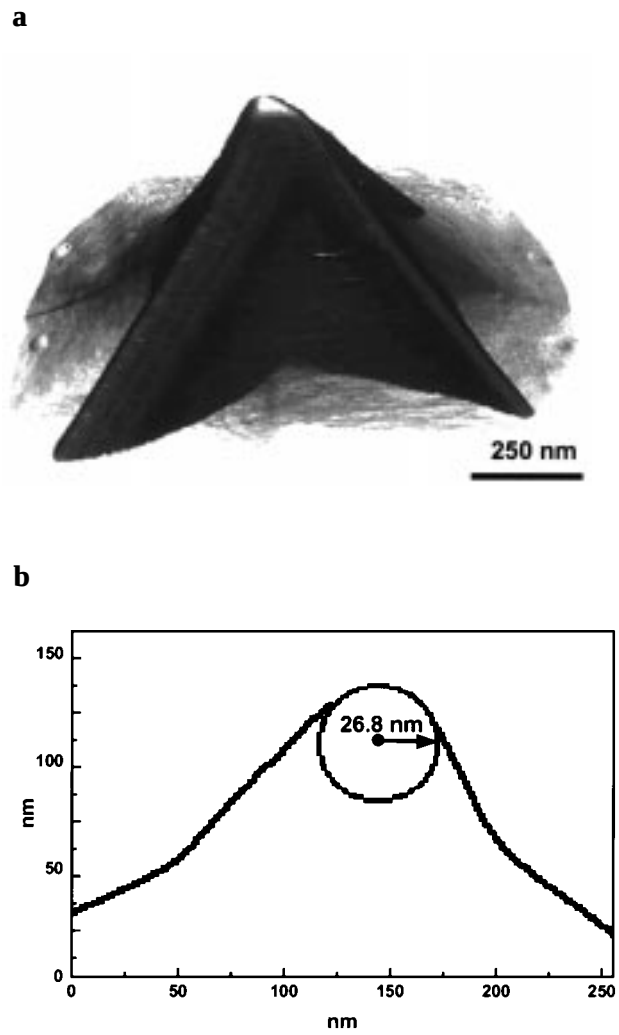

Figure 1. (a) Surface-rendered topographic AFM image of calibration grating displaying tip geometry. (b) Profile of calibration grating and radius of curvature measurement.

i.e., no discernible wear or roughening occurred. Applied forces were ≈10−15 nN, and tip−sample adhesive forces were ≈15−30 nN. The exact values of contact forces were evaluated for each experiment and used in the results and discussion sections.

The frictional force was determined from (one-half) the difference of trace (left-to-right) and retrace (right-to-left) 512 × 512-pixel lateral-force images, as indicated in Figure 2. We term the result "friction difference" images. Topographic contributions to the overall lateral force were independent of scanning direction, and thus were removed by the subtraction process. Hysteresis in the scanning position (from trace to retrace images) also was removed by invoking a 1−2 pixel shift between trace and retrace images, yielding a more precise removal of topographic contributions. Image subtraction and shifting was accomplished using customized image processing algorithms. The frictional force was quantified by creating "friction histograms" of friction difference images, i.e., the number of image pixels within incremental friction−force intervals.[14] This reduces 512 individual scan lines to a "spectroscopic" line shape, as shown in Figure 2, including information on the *distribution* of frictional forces. Images were collected with offset and planefit functions disabled, thereby retaining the zero of lateral force and thus the offset of the frictional peak on the friction force axis. All friction peaks were fit to a Gaussian distribution, as shown (Figure 2), to determine the mean value and breadth of the frictional force distribution. Numerous methods of friction force calibration exist;[20−22] absolute friction forces in our study were determined by utilizing the coefficient of friction for SiO_2 on SiO_2

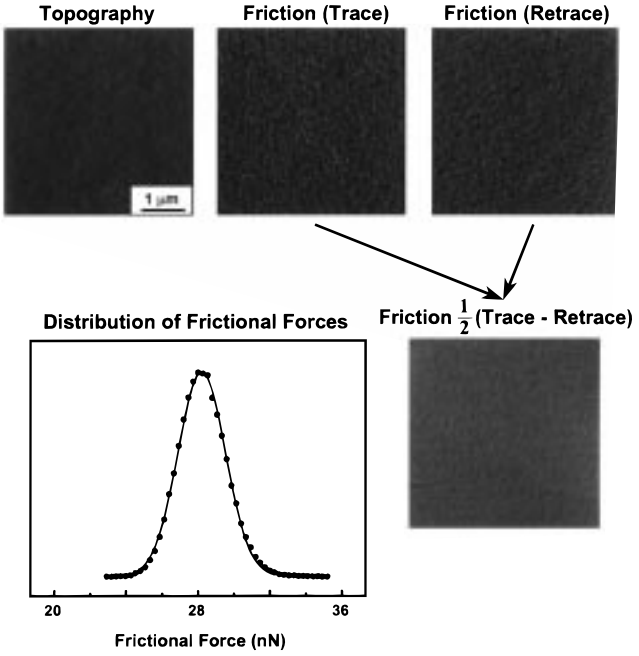

Figure 2. 4 μm × 4 μm topography, friction (trace), friction (retrace), and friction difference images of PMMA film surface. Histogram of friction difference image, fit to Gaussian distribution, displaying the distribution of frictional forces.

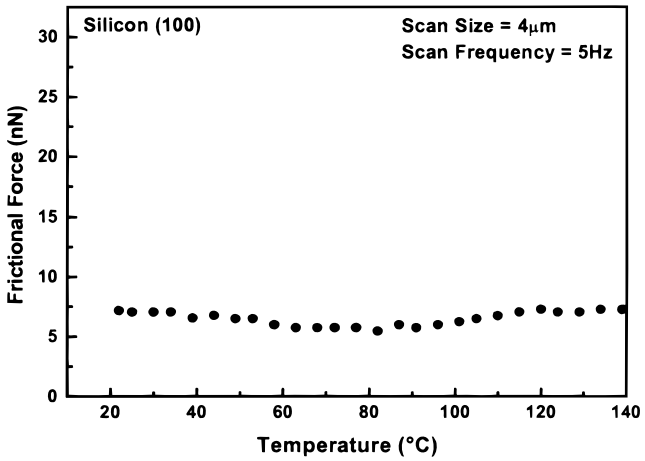

Figure 3. Mean frictional force vs temperature for a silicon (100) wafer with native oxide.

as a standard.[23] All temperature and velocity-dependent frictional data reported herein use one subtracted friction image (512 × 512-pixel trace-retrace) per data point. All images, except those used for the velocity/frequency variation study, used a scan size of 4 × 4 μm and scan frequency of 5 Hz, implying a scan velocity (2 × (scan width) × (scan frequency)) = 40 μm/s.

Force vs *Z* displacement ("force curve") measurements were collected several micrometers away from the imaged region prior to image collection. This procedure was repeated at each temperature, scan size, or frequency change in order to maintain a constant applied load and detect any changes in the state of the tip. Tip−sample adhesive (pull-off) forces are evaluated in the results section over the temperature range used in these experiments.

Figure 3 displays mean friction force as a function of temperature for a Si(100) wafer covered with native oxide. These data were collected as a control and exhibit no substantial temperature dependence within our experimental range. All reported variations in friction on polymers, as a function of temperature, are thus attributed to the properties of the material or its interaction with the SFM tip.

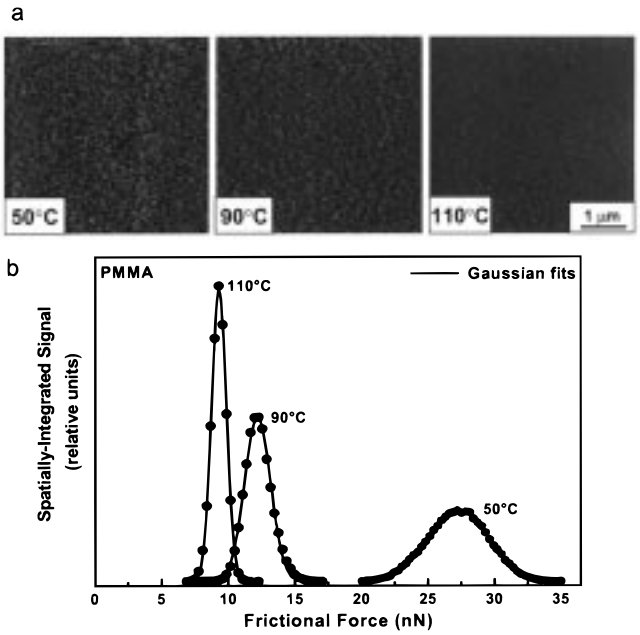

Figure 4. (a) Friction difference images at 50, 90, and 110 °C on a PMMA film surface. (b) Histograms of friction difference images, at different temperatures, and fit to Gaussian distribution.

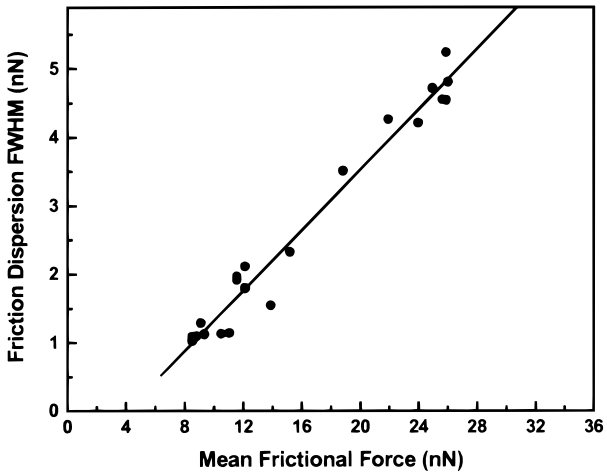

Figure 5. Friction histogram dispersion vs mean frictional force for a PMMA film surface.

Results

Temperature Dependence of Friction on PMMA, PET, and PS. The temperature dependence of friction on a PMMA film is shown in Figure 4. Friction difference images are displayed for three temperatures, 50, 90, and 110 °C (Figure 4a). All three images have the same *Z* (friction) scale and exhibit a "granular" frictional nanostructure. No noticeable change in nanostructure occurred in the topography with increasing temperature. Quantitative histograms of these images (Figure 4b) are symmetric and are effectively reproduced by a Gaussian function. The mean value and breadth of the distribution change dramatically as a function of temperature. Figure 5 shows a linear relationship between the dispersion (histogram width) and the mean value of friction determined in the 25−120 °C range. This relationship suggests the statistical nature of friction force measurements as follows. Some probability exists for small, discrete lossy events (relaxations) at each pixel location on a friction image. The more likely each

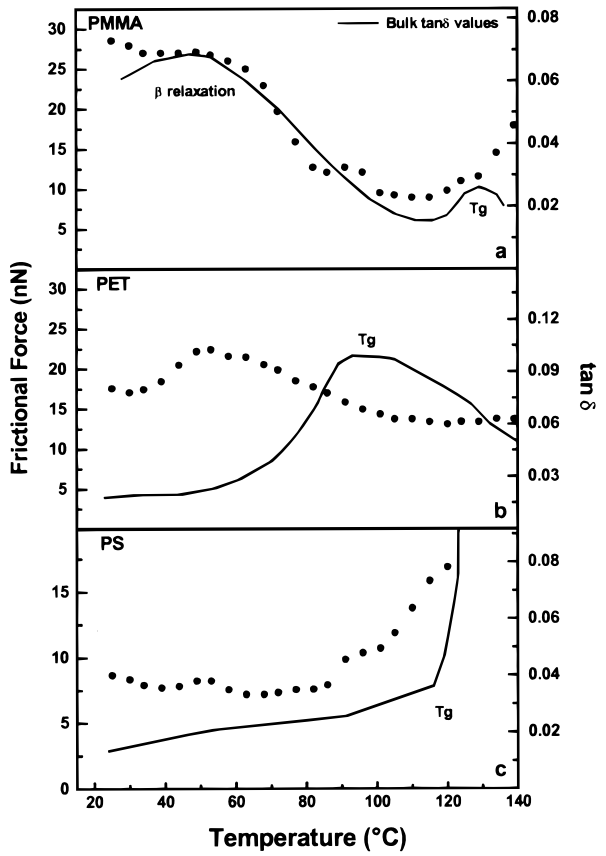

Figure 6. (a) Frictional force vs temperature for a PMMA film. (b) Frictional force vs temperature for a PET film. (c) Frictional force vs temperature for a PS film. Parts a−c were overlaid with literature bulk viscoelastic data.

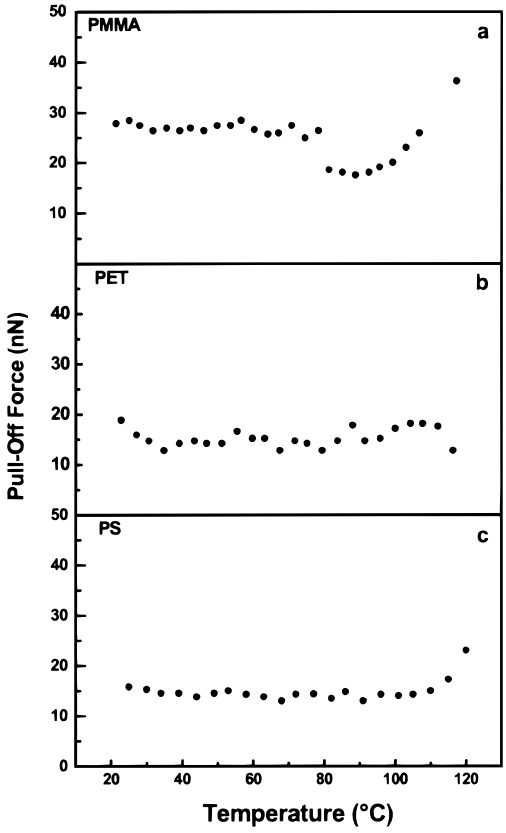

Figure 7. (a) Pull-off force (adhesive) vs temperature for a PMMA film. (b) Pull-off force (adhesive) vs temperature for a PET film. (c) Pull-off force (adhesive) vs temperature for a PS film. Data were obtained during Figure 6 friction data collection.

event (at certain temperatures) is, the greater the number of events that occur in the time interval of one pixel measurement. The more individual lossy events there are, the greater their sum and its variation between different measurements. Thus the distribution of measurements is a Gaussian relationship $y(F_f)$

$$y = \frac{A}{\sigma\sqrt{\pi/2}} e^{-2(F_f - \bar{F}_f)^2/\sigma^2} \quad (1)$$

where F_f is friction, $\bar{F}_f$ is the mean value, σ is the standard deviation, A is the area, and y is the magnitude. Work exploring the dispersion of frictional forces will be discussed in a future publication.

The mean values from representative friction histograms for PMMA, PET, and PS are plotted as a function of temperature in Figure 6a−c. For each polymer there is a characteristic, reproducible dependence on temperature. Friction data for PMMA displays a broad peak centered at ≈50 °C and another smaller peak is centered at ≈90 °C. In bulk viscoelastic studies the maximum of the secondary β molecular relaxation occurs at 50 °C at ≈2000 Hz.[24] The β mechanism is assigned to the hindered rotation of the $-COOCH_3$ group about the C−C bond linking it to the main polymer chain.[24] The glass to rubber transition (T_g), measured from bulk studies, for PMMA, PET, and PS at 2000 Hz are approximately 125, 95, and 125 °C, respectively.[24] In Figure 6a−c literature tan δ data at 2000 Hz are included for comparison and are shown as solid lines.[24] For each polymer there is good agreement with the overall shape of the measured friction and tan δ curves (Figure 6a−c). In particular, the breadth of the relaxation peaks (fwhh) are well correlated, except in the case of PS where the explored temperature interval includes only a monotonic rise of dissipation.

The pull-off force (a measure of adhesion) of the probe tip was measured for PMMA, PET, and PS at each temperature (Figure 7a−c) prior to collecting friction images. Figure 7a displays no temperature dependence on adhesion for PMMA until a temperature of 80 °C where a discontinuity results, most likely from a change in tip state, then a steady increase in pull-off force results as the temperature increases well into the rubbery regime. PET displays no temperature dependence in pull-off force throughout the full temperature range explored (Figure 7b). Figure 7c shows an increase in pull-off force beginning at 120 °C, which is above the bulk glass-transition temperature of PS.

Time−Temperature Dependence on Friction. The interplay between relaxation time and temperature, i.e., time−temperature superposition, is well-established in polymer studies.[17] In this investigation we focus upon PMMA to compare the dependencies of friction on scan velocity and temperature, and to relate the findings to molecular relaxations at the polymer surface. In Figure 8 the temperature dependence of friction is plotted with different symbols at four scanning velocities ranging from 2 to 220 μm/s as indicated. Velocities of 220, 50, 20, and 2 μm/s are achieved through increasing scan frequency and scan size. Data were acquired at all four velocities prior to ramping to the next temperature of interest. As rate decreases, the β relaxation peak (at 40 °C for 220 μm/s) apparently shifts to lower temper-

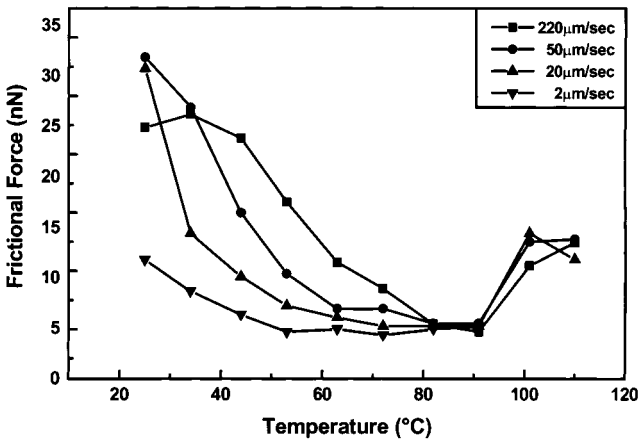

Figure 8. Frictional force vs temperature taken at 2, 20, 50, and 220 μm/s scan velocities for a PMMA film.

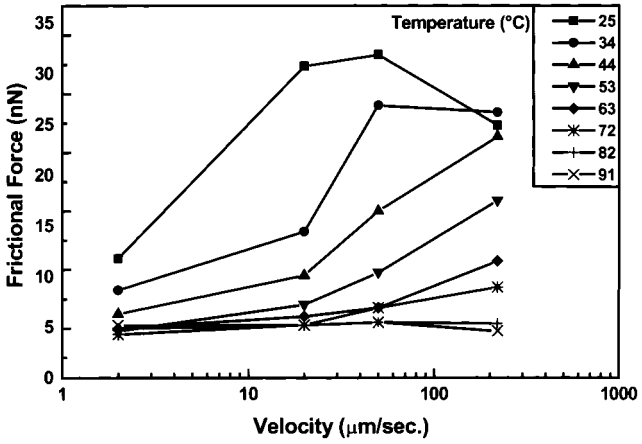

Figure 9. Frictional force vs scan velocity at several temperatures for a PMMA film.

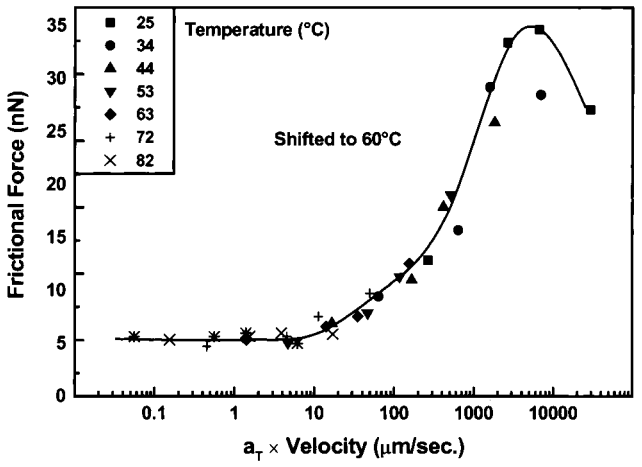

Figure 10. "Master curve" of frictional force vs velocity data shifted to 60 °C.

atures. This is consistent with the idea that the same molecular relaxation requires longer time at lower temperatures. Figure 9 is the same PMMA data from Figure 8 but plotted as friction vs velocity at discrete temperatures. Figure 10 shows a "master curve" constructed from the velocity-dependent data (Figure 9). Here each set of data (at a given temperature) is multiplied by a shift factor a_T, such that the data sets overlie each other.

The Arrhenius relationship (eq 2) between shift factor a_T, and temperature T is commonly used for secondary

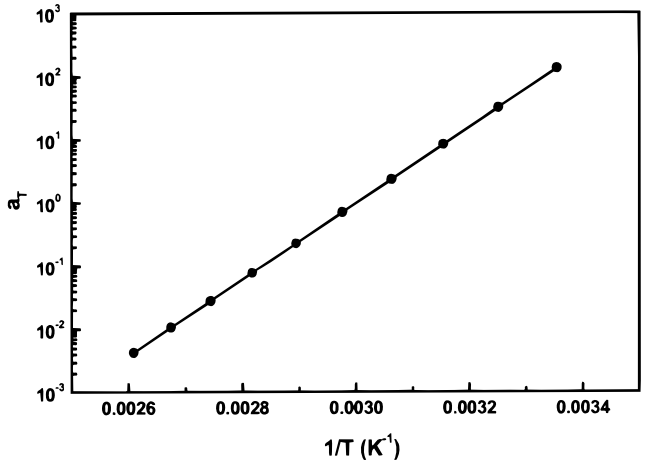

Figure 11. Arrhenius plot of shift factor a_T vs inverse temperature, with linear fit.

relaxation phenomena,[24] where T_0 is the reference

$$\ln a_T = \frac{E_a}{R}\left(\frac{1}{T} - \frac{1}{T_0}\right) \qquad (2)$$

temperature and E_a is the activation energy. In Figure 10 the velocities at different temperatures were shifted to a reference temperature of 60 °C. The Arrhenius plot of a_T vs $1/T$ is shown in Figure 11. From the slope of the Arrhenius plot, an activation energy of ≈12 kcal/mol was calculated for the hindered rotation of the $-COOCH_3$ in PMMA.

Discussion

Friction traditionally is described with two terms, interfacial ("adhesive") forces and "deformation" (mechanical loss) forces. It is important to consider both when interpreting results to assign a mechanism of friction. Figure 7 shows no increase in pull-off force (adhesion) except when the temperature is sufficiently high, into the rubbery regime. Above T_g the contact zone will increase because of a decrease in polymer modulus. In the case of PMMA, this increase in contact zone did not occur until well into the rubbery regime and very near the bulk glass transition temperature. PS displayed an increase in pull-off force very near the bulk T_g as well. PET showed no such increase, but most likely at much higher elevated temperatures it would display a similar increase in pull-off force. For the polymer films, studied herein, temperature-dependent changes in friction clearly relate to variations in mechanical (viscoelastic) loss. Given the minimal changes in adhesion with temperature, our interpretations clearly must focus upon mechanical energy dissipation.

Velocity/Frequency Relationship. The characteristic temperature-dependent line shapes for each polymer, as determined by bulk dynamic mechanical or dielectric experiments from literature,[24] were compared to our frictional measurements. For the comparison to be valid the literature data must match the friction data in the frequency (time scale) of the measurement. The conversion procedure of scan velocity to frequency has been described in a previous publication,[15] whereby a contact diameter was calculated to convert scan velocity to frequency by simple division. The contact diameter thus determines the time the probe tip affects a point on the polymer surface. Given a radius of curvature of

20 nm, applied load = 10 nN, and adhesive load = 15 nN and assuming a bulk storage modulus, the contact diameter can be estimated by JKR theory to be 18.7 nm. Thus for a scan velocity of 40 μm/s the equivalent frequency of measurement of ≈2000 Hz can be used for comparison to tabulated tan δ data acquired at this frequency.

It is important to consider possible errors in the comparison of time scales for tan δ and friction measurements. A potential difficulty of this analysis is its reliance on an estimate of the tip−sample contact diameter. Measurement of the radius of curvature of the tip involves either a calibration grating, as in our case, or SEM images of the tip. If the radius measured is under/overestimated by a factor of 2 the frequency calculated changes by the same amount, or $\approx 10^{0.3}$ Hz. For the polymers studied herein, a change of 1 order of magnitude in frequency corresponds to a relaxational peak shift of 5 °C. Thus our methodology should be within ≈1 °C of measured dynamic experiments, if no differences in surface and bulk properties existed. Furthermore, to account for the 35 and 50 °C differences between measurement types our rate conversion methodology would have to produce errors of 7 orders of magnitude in frequency for PMMA and 10 orders of magnitude in frequency for PET using 5 °C per order of magnitude shift in temperature for the time−temperature conversion for both polymers.[24] Although approximations certainly yield some error in our rate conversion, clearly they alone cannot account for such egregious differences in T_g. Of course the force field extending beyond the tip into the polymer must also be involved in the conversion. This will be addressed in the next section.

Friction/tan δ Relationship. To compare *absolute* values of tan δ and frictional force, a relationship must be developed. Several models correlating the loss tangent (tan δ) to frictional force on polymer surfaces have been proposed.[25] We present here an alternative model, which relies only on experimentally derived parameters. This will enable direct comparison between measured frictional forces and tabulated viscoelastic loss data.

To model a force microscope probe tip on a compliant flat surface we assume spherical-cap contact geometry. At this time, this is a necessary approximation, as there is no way to access the exact shape of the contact zone between tip and sample surface during a SFM experiment, this remains a difficulty in all SPM contact modeling. Justification for this assumption is shown in Figure 1b, whereby the tip apex measured for our probe tip was approximately spherical. When the sphere slides across a compliant sample it induces a trench-shaped deformation region (Figure 12). The amount of energy dissipated (δU) per sliding distance (δx) is the frictional force. As described in previous theories, the energy dissipated per unit volume of deformed polymer is described by the loss modulus E''.[25] Energy dissipation due to the breaking of interfacial adhesive bonds is ignored, because measured variations in friction are not tracked by variations in pull-off force. For a spherical tip with radius of curvature R, contact radius a, and spherical-cap cross section of area A, we obtain

$$F_f = \frac{\delta U}{\delta x} = \frac{E'' A \delta x}{\delta x} = E'' R^2 \left[\sin^{-1}\left(\frac{a}{R}\right) - \frac{a}{R}\sqrt{1 - \left(\frac{a}{R}\right)^2} \right] \quad (3)$$

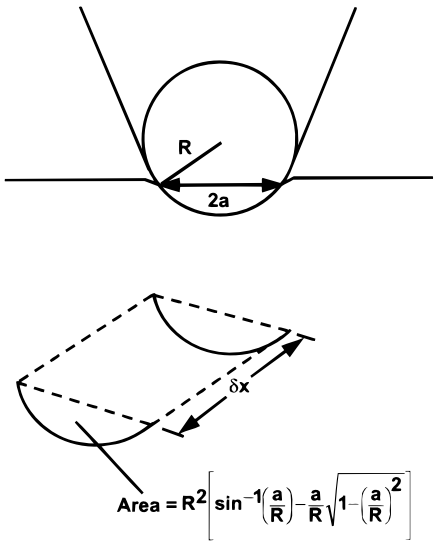

Figure 12. Diagram of probe tip on surface and volume element traced out by tip.

Expanding F_f in a power series of (a/R), using the first three terms of the expansion, we obtain:

$$F_f = E'' R^2 \left[\frac{2}{3}\left(\frac{a}{R}\right)^3 + \frac{1}{5}\left(\frac{a}{R}\right)^5 - \frac{3}{28}\left(\frac{a}{R}\right)^7 + ... \right] \quad (4)$$

We assume a JKR contact model,[26] whereby the contact radius is described by

$$a^3 = \frac{R}{K}\left[F_{ap} + 3\pi R W_{12} + \sqrt{6\pi R W_{12} F_{ap} + (3\pi R W_{12})^2} \right] \quad (5)$$

where F_{ap} is the applied force, W_{12} is the interfacial energy, and K is

$$K = \frac{4}{3}\left(\frac{1 - \mu_{polymer}^2}{E'_{polymer}} + \frac{1 - \mu_{tip}^2}{E'_{tip}} \right)^{-1} \quad (6)$$

where E' is the elastic modulus and μ is the Poisson ratio. The JKR equation is substituted for a/R and simplified, where

$$x = F_{ap} + 3\pi R W_{12} + \sqrt{6\pi R W_{12} F_{ap} + (3\pi R W_{12})^2} \quad (7)$$

We substitute for a/R in eq 4 to obtain

$$F_f = E'' R^2 \left[\frac{2}{3}\left(\frac{x}{R^2 K}\right) + \frac{1}{5}\left(\frac{x}{R^2 K}\right)^{5/3} - \frac{3}{28}\left(\frac{x}{R^2 K}\right)^{7/3} + ... \right] \quad (8)$$

Equation 8 simplifies to obtain the tan δ dependence on friction.

$$F_f = \frac{2xK'}{3}\frac{E''}{E'} + \frac{R^2 E''}{5}\left(\frac{xK'}{R^2 E'}\right)^{5/3} + ... = x \tan\delta \left[\frac{2K'}{3} + \frac{1}{5}\left(\frac{xK'}{R^2 E'}\right)^{2/3} + ... \right] \quad (9)$$

where $K' = E'/K$. The second term in the expansion accounts for <10% of the overall friction calculated from eq 9, given the R, W_{12}, and applied loads used in our experiments; higher order terms contribute even less. Equation 9 adequately accounts for the dependence of

friction on temperature through most of the range presently explored. At temperatures up to T_g the temperature dependence of the loss modulus dominates the frictional response. Above the glass transition a presumed decrease in storage modulus increases the contact area thereby increasing the adhesive component of friction (Figure 7a,c).

The largest source of error in this model is the assumption that the volume element for dissipation only includes the amount of polymer traced out by the probe tip. In actuality additional energy will be dissipated by creation of a strain field which extends farther into the polymer. To gauge the contact volume involved in the friction measurement we use eq 8 to estimate the difference between friction and tan δ with this model. Taking literature tan δ values for the 3 polymer systems as being 0.03, 0.10, and 8 for PMMA, PET, and PS α relaxations (T_g), and 0.068 for the β relaxation in PMMA, we can calculate a frictional force through the use of eq 9.[24] Knowing the radius of curvature of the tip and the interfacial energy (a function of the adhesive force measured in our experiments), we calculate the frictional forces as 5.4 nN and 2.4 nN for PMMA β and α relaxations and 3.8 nN for the PET α relaxation. PS cannot be evaluated due to the lack of a maximum in frictional force for the T_g. Thus our model underestimates friction by a factor of $\approx$5 for all three relaxations. If we calculate the ratio of (a/R) needed to account for the measured frictional forces a value of $\approx$0.80 is obtained. If in fact the contact radius was a large portion of the radius of curvature, wear into the film would be expected, especially since the film is on the order of R. Thus a strain field extending farther into the polymer film, beyond the probe tip is likely. If we use this larger deformation diameter in our velocity to frequency conversion the result is an effective shift of relaxation peaks to a slightly lower temperature. Clearly the T_g depression implied in our results is real.

Thin Film/Bulk Comparison. In all surface friction studies, we observe the position of the glass-transition temperature lowered somewhat compared to bulk dynamic mechanical measurements. The friction data for PMMA and PET contain peaks corresponding to tan δ peaks, but shifted 35 and 50 °C lower, respectively. Furthermore the activation energy of $\approx$12 kcal/mol calculated for the hindered rotation of the $-COOCH_3$ in PMMA was lower than the previously measured value (17−23 kcal/mol) using bulk mechanical and dielectric methods.[24] Although the position of the β relaxation in PMMA (Figure 6a) corresponds to the bulk value, this lowered activation energy would suggest otherwise. Most likely the discrepancy arises from the previously discussed underestimated contact zone which would lower the comparison frequency of the measurement.

The lowered T_g and rotational activation energies may be indicative of a greater free volume at the polymer surface. Depression of the glass transition has been observed for films similar in thickness to ours (<100 nm).[3,6,7] The effect has been attributed to an increase in free volume in the polymer due to the effects of constraining surfaces. This affects the polymer conformations and such effects could account for the drastic departure from bulk behavior observed in the present study. It is also known that elevated pressure under the probe could *increase* the glass transition temperature,[27−29] but the magnitude of such an effect may be quite small under the relatively low contact forces ($\approx$20 nN) examined in this work. Research into issues of substrate interaction, thickness, and pressure is ongoing.

Conclusions

A quantitative method, using temperature controlled FFM and "friction histograms," has been developed to determine the frictional (dissipative) character of polymer surfaces. The use of two-dimensional friction images containing 512 scan lines as opposed to one-dimensional friction loops enabled efficient data collection and high signal/noise determination of the *distribution* of frictional forces. It was found that the mean value and dispersion of frictional forces vary with temperature. Dispersion increases in proportion to increasing mean value. This suggests a statistical nature in even nanometer-scale friction measurements, each image pixel representing the sum of many discrete lossy events (relaxations).

Our method allowed us to correlate frictional response in films of PMMA, PET, and PS with known α and/or β relaxation mechanisms. With every polymer systems we observed a marked shift of the glass-transition temperature (peak in friction) to lower temperatures compared to bulk measurements (peak in tan δ). The temperature of the β relaxation in PMMA via FFM was consistent with bulk tan δ measurements. The rate dependence of this relaxation was consistent with Arrhenius time−temperature behavior allowing calculation of an activation energy. The activation energy was lower than measured bulk values. Together with depressed T_g values, this suggests greater mobility at the polymer surface.

The magnitude of measured frictional force and tabulated tan δ values differed by a constant factor when related via a spherical deformation model. This suggests that the volume probed by the tip may be several times greater than estimated in the JKR model.

Acknowledgment. This work was supported by grants from the Center for Interfacial Engineering and the donors of the Petroleum Research Fund, administered by the American Chemical Society. We also wish to thank Molecular Imaging for their technical support.

References and Notes

(1) Feast, W. J.; Munro, H. S.; Richards, R. W. *Polymer Surface and Interfaces*; Wiley: New York, 1993; Vol. 2.
(2) Garbassi, F.; Morra, M.; Occhiello, E. *Polymer Surfaces*; John Wiley and Sons: West Sussex, England, 1994.
(3) Keddie, J. L.; Jones, R. A. L.; Cory, R. A. *Europhys. Lett.* **1994**, *27*, 59.
(4) Kajiyama, T.; Tanaka, K.; Takahara, A. *Macromolecules* **1997**, *30*, 280.
(5) Forrest, J. A.; Dalnoki-Veress, K.; Dutcher, J. R. *Phys. Rev. E* **1997**, *56*, 5705.
(6) Forrest, J. A.; Dalnoki-Veress, K.; Stevens, J. R.; Dutcher, J. R. *Phys. Rev. Lett.* **1996**, *77*, 2002.
(7) Keddie, J. L.; Jones, R. A. L.; Cory, R. A. *Faraday Discuss.* **1994**, *98*, 219.
(8) DeMaggio, G. B.; Frieze, W. E.; Gidley, D. W.; Zhu, M.; Hristov, H. A.; Yee, A. F. *Phys. Rev. Lett.* **1997**, *78*, 1524.
(9) Mayes, A. M. *Macromolecules* **1994**, *27*, 3114.
(10) Affrossman, S.; Hartshorne, M.; Jermone, R.; Pethrick, R. A.; Petitjean, S.; Vilar, M. R. *Macromolecules* **1993**, *26*, 6251.
(11) Grosch, K. A. *Proc. R. Soc. London* **1963**, *274*, 21.
(12) Ludema, K. C.; Tabor, D. *Wear* **1966**, *9*, 329.
(13) Overney, R. M.; Meyer, E.; Frommer, J.; Brodbeck, D.; Lüthi, R.; Howald, L.; Güntherodt, H.-J.; Fujihira, M.; Takano, H.; Gotoh, Y. *Nature* **1992**, *359*, 133.

(14) Haugstad, G.; Gladfelter, W. L.; Weberg, E. B.; Weberg, R. T.; Jones, R. R. *Langmuir* **1995**, *11*, 3473.
(15) Hammerschmidt, J. A.; Moasser, B.; Gladfelter, W. L.; Haugstad, G.; Jones, R. R. *Macromolecules* **1996**, *29*, 8996.
(16) Tanaka, K.; Takahara, A.; Kajiyama, T. *Macromolecules* **1997**, *30*, 6626.
(17) Ferry, J. D. *Viscoelastic Properties of Polymers*; Wiley & Sons: New York, 1980.
(18) Bustamante, C.; Keller, D. J. *Phys. Today* **1995**, *48*, 32.
(19) Biscarini, F.; Levy, P. *Appl. Phys. Lett.* **1997**, *71*, 888.
(20) Noy, A.; Frisbie, C. D.; Rozsnyai, L. F.; Wrighton, M. S.; Leiber, C. M. *J. Am. Chem. Soc.* **1995**, *117*, 7943.
(21) Putman, C.; Igarashi, M.; Kaneko, R. *Jpn. J. Appl. Phys.* **1995**, *34*, L264.
(22) Ogletree, D. F.; Carpick, R. W.; Salmeron, M. *Rev. Sci. Instrum.* **1996**, *67*, 3298.
(23) Overney, R. M.; Buenviaje, C. *Polymer Preprints* **1998**, *39*, 1143.
(24) McCrum, N. G.; Read, B. E.; Williams, G. *Anelastic and Dielectric Effects in Polymeric Solids*; Wiley: London, 1967.
(25) Moore, D. F. *The Friction and Lubrication of Elastomers*; Pergamon Press: Ltd.: Oxford, England, 1972.
(26) Johnson, K. L.; Kendall, K.; Roberts, A. D. *Proc. R. Soc. London A* **1971**, *324*, 301.
(27) Billinghurst, P. R.; Tabor, D. *Polymer (G.B.)* **1971**, *12*, 101.
(28) Parry, E. J.; Tabor, D. *Polymer (G.B.)* **1973**, *14*, 617.
(29) Stevens, J. R.; Coakley, R. W.; Chau, K. W.; Hunt, J. L. *J. Chem. Phys.* **1985**, *84*, 1006.

MA981966M